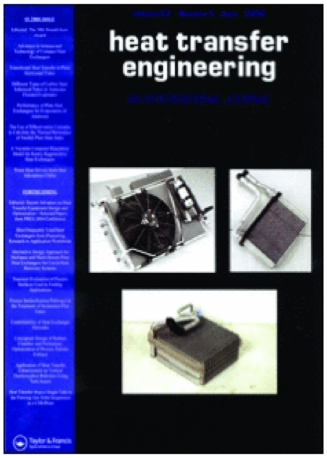

Heat Transfer Engineering
Publication details, including instructions for authors and subscription information:
http://www.informaworld.com/smpp/title~content=t713723051

On the Prediction of Heat Transfer in Micro-Scale Flow Boiling

Gherhardt Ribatski [a]; Wei Zhang [b]; Lorenzo Consolini [a]; Jinliang Xu [b]; John R. Thome [a]
[a] Laboratory of Heat and Mass Transfer, École Polytechnique Fédérale de Lausanne, Lausanne, Switzerland
[b] Micro Energy System Laboratory, Guangzhou Institute of Energy Conversion, Guangzhou City, China

Online Publication Date: 01 October 2007
To cite this Article: Ribatski, Gherhardt, Zhang, Wei, Consolini, Lorenzo, Xu, Jinliang and Thome, John R. (2007) 'On the Prediction of Heat Transfer in Micro-Scale Flow Boiling', Heat Transfer Engineering, 28:10, 842 - 851
To link to this article: DOI: 10.1080/01457630701378267
URL: http://dx.doi.org/10.1080/01457630701378267

Heat Transfer Engineering, 28(10):842–851, 2007

ISSN: 0145-7632 print / 1521-0537 online
DOI: 10.1080/01457630701378267

On the Prediction of Heat Transfer in Micro-Scale Flow Boiling

GHERHARDT RIBATSKI
Laboratory of Heat and Mass Transfer, École Polytechnique Fédérale de Lausanne, Lausanne, Switzerland

WEI ZHANG
Micro Energy System Laboratory, Guangzhou Institute of Energy Conversion, Guangzhou City, China

LORENZO CONSOLINI
Laboratory of Heat and Mass Transfer, École Polytechnique Fédérale de Lausanne, Lausanne, Switzerland

JINLIANG XU
Micro Energy System Laboratory, Guangzhou Institute of Energy Conversion, Guangzhou City, China

JOHN R. THOME
Laboratory of Heat and Mass Transfer, École Polytechnique Fédérale de Lausanne, Lausanne, Switzerland

Xu et al. have recently published a set of results for boiling heat transfer measurements in a multi-channel micro-scale evaporator for flow boiling of acetone in triangular cross-section channels (hydraulic diameter of 155.4 mm). In the present collaboration, we assess our current capability to predict this independent flow boiling data set with a fluid not in the original database and also much smaller in size using the phenomenological three-zone model of Thome, Dupont, and Jacobi. The method models boiling in small diameter channels in the elongated bubble/slug flow regime. The boiling data falling in this regime are identified here using a new micro-scale flow pattern map proposed by Revellin in order to utilize only test data corresponding to the elongated bubble flow mode. The decrease of the measured wall temperature due to the heat spread by longitudinal conduction through the heat sink was investigated through a finite differences analysis. In addition, a data reduction procedure different than that one used by Xu et al. was used and, consequently, some differences in the heat transfer behavior were found. Based on the present database, a new set of empirical parameters for the three-zone model was proposed. The conjugated effect of flow pattern and bubble/slug frequency on the heat transfer coefficient was also investigated.

INTRODUCTION

Two-phase compact heat exchangers with micro-scale channels possess clear advantages over those with macro-scale channels, also referred to as conventional channels in the literature. Micro-scale channels can endure a higher operating pressure and provide a much larger contact area with fluid per unit volume than large tubes. Furthermore, they seem to present much higher heat transfer coefficients at similar operating conditions. These advantages favor the development of extremely compact heat exchangers in order to minimize the size and amount of material used in their manufacture, as well as the refrigerant inventory used in the system. The high degree of compactness yields new application areas for such devices, which increase as they advance to smaller sizes. However, two-phase heat exchanger cooling devices (evaporators) are being developed in a heuristic way without the benefit of proven thermal design methods for predicting their heat transfer and pressure drops. In fact, as pointed out by Thome [1], the technologies available for the miniaturization of micro-cooling devices (evaporators and condensers) have vastly outpaced what can be hydraulically and thermally modeled.

Address correspondence to Dr. Gherhardt Ribatski, Dept. Engenharia Mecânica, Escola de Engenharia de São Carlos, Universidade de São Paulo (USP) Av. Trabalhador San-carlense, 400, 13566-970, São Carlos-SP, Brazil. E-mail: ribatski@sc.usp.br

Recently, Thome et al. [2] proposed a micro-scale model that is comprised of three heat transfer zones and in particular describes the evaporation of elongated bubbles. Ribatski et al. [3], based on a comparison of current heat transfer prediction methods [2,4,5] and a broad database from the literature that included more than 2000 data points, suggested that this seems to be the most promising approach. Such a conclusion was based on the fact that this method, when integrated with a reliable micro-scale flow pattern map characterizing the elongated bubble flow patterns, may provide a more complete scenario of the heat transfer process in micro-scale channels and has the potential to lead to a reliable design tool. Furthermore, a physically based model can also be used to investigate dynamic effects (such as temporal or local variations in heat flux on heat transfer) while wholly empirical methods [4,5] cannot. Agostini and Thome [6] have shown that the three-zone model predicts reasonably well in the Agostini [7] database that falls in the elongated bubble flow regime.

Recently, a new flow pattern prediction method has been proposed by Revellin [8] for convective evaporation inside micro-scale channels for tests with R134a and R245fa in 0.5 and 0.8 mm channels. This method is based on flow images from a high-speed digital camera coupled with the analysis of the intensity of laser beams crossing a glass tube within the testing fluid. The glass tube had the same internal diameter as the evaporating section and was located just after it.

In this paper, the flow pattern prediction method proposed by Revellin [8] is used for the first time to segregate independent experimental heat transfer data according to different micro-scale flow patterns. The heat transfer data were obtained for evaporating acetone in a micro-scale multi-channel evaporator at the Micro Energy System Laboratory at the Guangzhou Institute of Energy Conversion in China. The data corresponding to the elongated bubble flow regime is compared against the predictions of the three-zone model. Finally, new values for the experimental parameters in the three-zone model were optimized specifically for the present database.

BRIEF DESCRIPTION OF THE THREE-ZONE MODEL

The micro-scale heat transfer model proposed by Thome and coworkers predicts the transient variation in local heat transfer coefficient during the cyclic passage of a liquid slug, t_l; an evaporating elongated bubble, t_{film}; and a vapor slug when present, t_v. A representation of the model is shown in Figure 1. In this figure, L_p is the total length of the pair or triplet, L_l is the length of the liquid slug, L_v is the length of the bubble including the length of the vapor slug with a dry wall zone L_{dry}, and L_{film} is the length of the liquid film trapped by the bubble. The internal radius and diameter of the tube are R and d, respectively, while δ_0 and $\delta_{\min}$ are the thicknesses of the liquid film trapped between the elongated bubble and the channel wall at its formation and at dryout. A time-averaged local heat transfer coefficient, α, during the period, τ, of the cycle is obtained according to the following

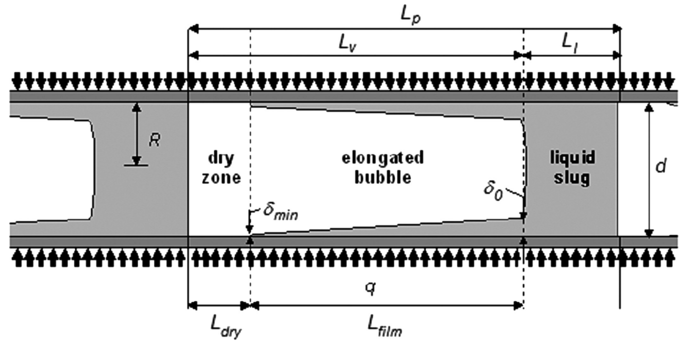

Figure 1 Diagram illustrating a triplet comprised of a liquid slug, an elongated bubble and a vapor slug in the 3-zone heat transfer model [2].

equation:

$$\alpha(z) = \frac{t_l}{\tau}\alpha_l(z) + \frac{t_{film}}{\tau}\alpha_{film}(z) + \frac{t_v}{\tau}\alpha_v(z) \tag{1}$$

In this expression, α_l and α_v are the heat transfer coefficients of the liquid and vapor slugs. They are calculated from their local Nusselt number using the London and Shah [9] correlation for laminar flow and the Gnielinski [10] correlation from transitional and turbulent flow. The Churchill and Ugasi [11] asymptotic method was used to obtain a continuous expression of the mean heat transfer coefficient as a function of Reynolds number. The time periods in Eq. (1) are determined as follows:

$$t_l = \frac{\tau}{1+\frac{\rho_l}{\rho_v}\frac{x}{1-x}}, \quad t_v + t_{film} = \frac{\tau}{1+\frac{\rho_v}{\rho_l}\frac{1-x}{x}}, \quad \tau = \left(\frac{c_q p_r^{n_q}}{q}\right)^{n_f},$$

and

$$t_{dryfilm}(z) = \frac{\rho_l h_{lv}}{q}[\delta_0(z) - \delta_{\min}] \tag{2}$$

where $t_{dryfilm}$ is the maximum duration of the existence of the film at position z and is used to evaluated the presence of the vapor slug. If $t_v + t_{film}$ given by Eq. (2) is greater than $t_{dryfilm}$, local dryout occurs (i.e., the liquid film thickness achieves the minimum feasible film thickness, $\delta_{end}(z) = \delta_{\min}$, and $t_{film} = t_{dryfilm}$). However, if $t_v + t_{film} < t_{dryfilm}$, then no dryout occurs since the next liquid slug arrives before the film dryout. This implies that $t_v = 0$, and the film thickness at the end of the evaporating time is given by:

$$\delta_{end}(z) = \delta(z, t_{film}) = \delta_0(z) - t_{film}\frac{q}{\rho_l h_{lv}} \tag{3}$$

In a companion paper to [2], Dupont et al. [12] proposed the following values for the set of experimental parameter in Eq. (2) by using a least square method and based on a database extracted from the literature: $\delta_{\min} = 0.3 \times 10^{-6}$ m, $c_q = 3328$ W/m^2 K, $n_q = -0.5$, and $n_f = 1.74$.

The mean heat transfer coefficient in the film is calculated by using the average value of the film thickness [12] during t_{film} according to:

$$\alpha_{film}(z) = \frac{2k_l}{\delta_0(z) + \delta_{end}} \tag{4}$$

To calculate the initial film thickness, the authors added an empirical correction factor, $C_{\delta 0}$, (equal to 0.29 in [12]) to the liquid film prediction method proposed by Moriyama and Inoe [13]:

$$\frac{\delta_0}{d} = C_{\delta 0}\left(\sqrt[3]{\frac{\mu_l}{U_p d \rho_l}}\right)^{0.84}\left[(0.07Bo^{0.41}) + 0.1^{-8}\right]^{-1/8},$$

$$U_p = G\left[\frac{x}{\rho_v} + \frac{1-x}{\rho_l}\right], \quad Bo = \frac{\rho_l d}{\sigma}U_p^2 \tag{5}$$

where U_p is the velocity of the pair (or triplet) liquid and vapor slug (homogeneous flow assumption) and Bo is the Bond number.

The original set of experimental parameters ($\delta_{\min}$, c_q, n_q, n_f, and $C_{\delta 0}$) were obtained based on an experimental database including 1591 test data taken from seven independent studies covering hydraulic diameters from 0.77 to 3.1 mm, heat fluxes from 9.8 to 178 kW/m^2, mass velocities from 50 to 564 kg/m^2 s, reduced pressures from 0.036 to 0.78, and vapor qualities up to 0.99 for the following seven fluids: R11, R12, R113, R123, R134a, R141b, and CO_2. Their general empirical constants are used in this comparison. This model predicted 70% of its original database to within ±30%.

FLOW PATTERN TRANSITION PREDICTION METHOD

The prediction method developed by Revellin [8] is used here to segregate the experimental data according to micro-scale flow patterns. This method comprises the following four distinct flow patterns:

1. isolated bubble flow, including bubbly flow and isolated slug flow,
2. coalescing bubble flow, where bubble and/or slug coalescence is observed and the slug frequency is not only a function of heat flux as assumed by the three-zone model,
3. annular flow, where liquid flows on the wall with a continuous vapor core in the center of the channel, and
4. post-dryout flow that is characterized by a dry surface with liquid droplets flowing in the vapor core.

Figure 2 illustrates a flow pattern map based on the criteria by [8]. According to this method, heat flux affects just the transition between isolated bubble and coalescing bubble flow. For the present experimental conditions, post-dryout flow would appear just at heat fluxes higher than 0.8 MW/m^2. Finally, based on the fact that the three-zone model was developed to predict heat transfer coefficients just in the presence of vapor slugs, neither the post-dryout flow nor the annular flow heat transfer data were considered here in this study.

EXPERIMENTAL FACILITY

The experimental campaign of which the results are presented in this paper was performed at the Micro Energy System Laboratory at the Guangzhou Institute of Energy Conversion in China. A detailed description of the experimental facility is found in Xu et al. [14,15]; thus, just a brief description is presented here.

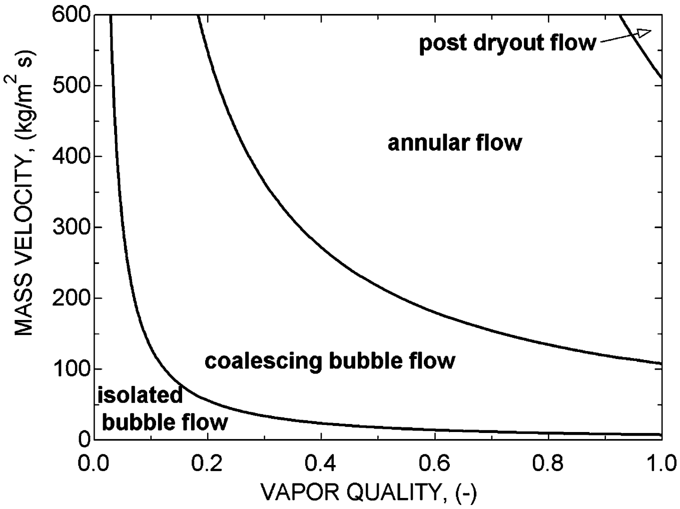

Figure 2 Flow pattern map based on the prediction method by Revellin [8]. Acetone, $D_{eq} = 0.201$ mm, $q = 300$ kW/m^2, $T_{sat} = 60°$C, test section length of 16 mm and no liquid subcooling.

Heat Sink Description

The heat sink was fabricated in silicon and was 30 mm in length, 7 mm in width, and 530 mm thick. Ten parallel triangular channels (300 µm wide, b, and 212 µm deep, h) with a pitch distance of 150 µm were centrally etched on the silicon substrate. Figure 3 shows a schematic diagram of the parallel silicon multi-channel micro-scale heat sink. The overall area within the channels is 21.450 mm in length and 4.350 mm in width. A glass cover was bonded with the silicon wafer, allowing

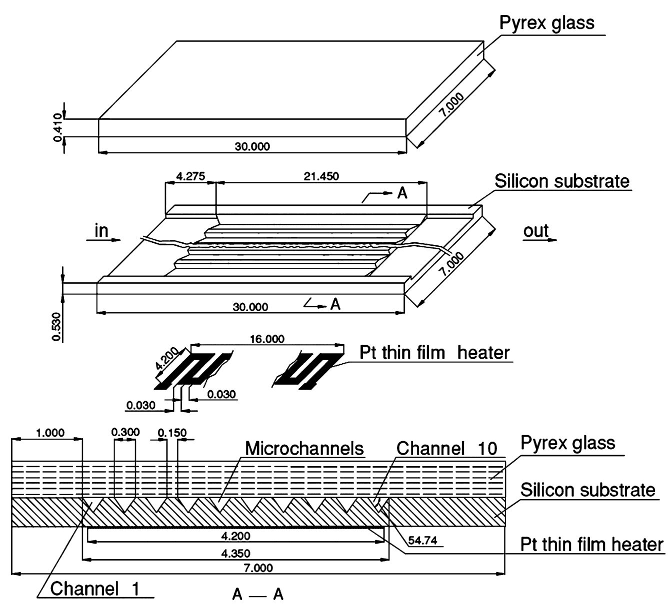

Figure 3 Schematic diagram of the multi-channel micro-scale test section.

high-speed flow visualizations, which are presented in Xu et al. [14,15].

On the backside of the heat sink, a thin platinum film was deposited with the same length as the channels. For a safe operation, the width of the film was 4.200 mm, which was narrower by half a triangular channel width. The effective heating length of the film was 16.000 mm, L_h, forming an effective heating area of 16.000 × 4.200 mm^2. Such an area was also the target for the infrared image temperature measurements. A very thin black lacquer was painted on the surface of the heating film in order to improve the IR temperature readings. An electrical power supply that provided AC current to the platinum film was used to impose a uniform heat flux on the backside surface of the heat sink.

Experimental Setup

In the experimental apparatus, pure liquid acetone (purity >99.5%) pressurized by nitrogen gas was driven from a tank, successively through a valve, 2 μm filters, the test section, a condenser, and then to a liquid container. A pressure control valve located between the nitrogen gas tank and the acetone reservoir was used to establish the pressure at the inlet of the test section. A PID temperature controller unit was used to set the temperature of the acetone in the reservoir, thus determining the temperature of the liquid acetone entering the test section. The fluid temperatures at inlet and outlet of the test section were measured by sheathed thermocouples. A pressure transducer was used to measure the pressure of the liquid at the inlet of the test section. The liquid mass flow rate was measured with a high precision balance according to the increase of liquid mass in the liquid reservoir over a period of time. Pressure and temperature signals were acquired by a HP acquisition system. An infrared camera (FLIR ThermaCAM SC3000 IR) was used to measure the heat sink temperature on the thin film on backside of the heat sink at steady-state conditions. This system has a thermal sensitivity of 0.02°C at 30°C, a spatial resolution of 1.1mrad and typical resolution of 320 × 240 pixels over the focused area. A PC connected to the IR imaging system stored the image files. The IR camera was centrally located so that the heating area of the heat sink was in the view field.

DATA REDUCTION PROCEDURE

A data reduction analysis is needed to calculate the local heat transfer coefficient and vapor quality along the test section. However, before the description of the adopted procedure, some comments on the definition of the mass velocity and heat flux should be made. In the present paper, G is defined as the total mass flow rate divided by the free cross-sectional area of the heat sink, which is 10 times the cross-sectional area of a single triangular channel. For the heat flux, the following different definitions may be adopted:

- Heat flux referred to the base area of the heat sink. In this definition, the heat flux dissipated by the heat sink is similar to the heat generated by the cooled device divided by the contact area. This is useful in a comparative analysis when the overall cooling capacities of different heat sinks are evaluated for a specific application. However, when used to estimate α, this definition restricts the experimental data to the tested cooling device and may lead to misinterpretations.
- Heat flux referred to the heated area in contact with the evaporating fluid. This definition was used by Xu et al. [14,15] and, from a phenomenological point of view, seems to be the most suitable procedure. However, in this case, a heat transfer model should account for the channel format and the heated perimeter. This may either restrict the model to a specific geometry or increase tremendously its complexity.
- Heat flux referred to the internal area of the channel based on the equivalent diameter. In this case, it is assumed that the channel is circular with an internal diameter (equivalent diameter, D_{eq}) yielding the same cross-sectional area as the real channel. The heat flux is given by the ratio of the dissipated heat and $N\pi D_{eq}L_h$, where N is the number of channels. Using this definition, a heat transfer prediction method like the three-zone model developed for a circular channel can be used for a non-circular channel without major modifications and, contrary to what occurs when using the hydraulic diameter, the flow velocity is kept the same. However, by adopting this procedure, non-circularity effects are neglected, such as the decreasing of the film thickness with a consequent increase in the local α, in the region between corners due to surface tension effects.

In this paper, the third definition was adopted, as the three-zone model was developed assuming a uniformly heated circular channel [2]. In addition, the flow pattern prediction method developed by Revellin [8], used to segregate the experimental data, was also based on results for circular channels. Thus, to calculate the heat flux, it is assumed that the heat sink is comprised of 10 uniformly heated circular channels, each having the same cross-sectional area as the original triangular channels. The heat flux is given by:

$$q = \frac{\varphi V I}{10 L_h \sqrt{2\pi h b}} \tag{6}$$

where V and I are the tension and current applied to the film heater, and φ is the ratio of the heat received by the fluid to the total heating power and was experimentally evaluated equal to 0.84 [14].

Based on the fact that subcooled liquid is supplied to the test section, the following procedures were adopted to calculate the fluid temperature along the heated length.

Fluid Subcooled Region

The subcooled region length, L_{sp}, and the saturation temperature and pressure at $z = L_{sp}$ were estimated from the simultaneous solution of an equation presented by [16] relating p_{sat} to T_{sat} plus the following equations:

$$(\varphi VI)\frac{L_{sp}}{L_h} = 5G(bh)C_l(T_{sat} - T_{in}) \tag{7}$$

$$p_{in} - p_{sat} = \frac{f}{2\rho_l}\frac{L_{sp}}{D_h}G^2 \tag{8}$$

where f is the friction factor given according to Shah and London [17] by $f = 13.311/Re_l$. Here, the hydraulic diameter was used to estimate the pressure drop in the single-phase region. The following linear liquid temperature distribution along the flow direction is assumed:

$$T_f(z) = T_{in} + \frac{z}{L_{sp}}(T_{sat} - T_{in}) \tag{9}$$

Fluid Saturated Region

A linear evaporating fluid temperature was also assumed here with T_f being estimated as follows:

$$T_f(z) = T_{sat} - \left[(T_{sat} - T_{out})\left(\frac{z - L_{sp}}{L_h - L_{sp}}\right)\right] \tag{10}$$

The local vapor quality and heat transfer coefficient are calculated, respectively, according to the local saturation temperature:

$$x(z) = \frac{C_l(T_{in} - T_{sat}) + \frac{[z(\varphi VI)]}{[5G(bh)L_h]}}{h_{lv}} \tag{11}$$

$$\alpha(z) = \frac{q}{T_{wall}(z) - T_f(z)} \tag{12}$$

where $T_{wall}(z)$ is the average wall temperature measured from two longitudinal centerlines on the heat sink at a z distance from the beginning of the heating length. Such a procedure was adopted in order to minimize effects of lateral conduction through the heat sink on the measured T_{wall}. According to Eq. (11), it should be also noted that negative values for the vapor quality are related to subcooled liquid. A saturation temperature of about 61°C was found for most of the experimental tests.

Thermodynamic and transport properties of acetone were evaluated locally according to the equations provided by Yaws [16]. Instruments were calibrated, and the uncertainties of the measured and calculated parameters are summarized in Table 1. The uncertainty in the heat flux does not include uncertainties in the estimation of heat losses.

HEAT TRANSFER DATA ANALYSIS

The experimental results are shown in Figure 4. For all experimental conditions, it can be noted that initially the heat transfer coefficient increases drastically with increasing vapor quality passing through a peak at x just below 0. After this maximum, further increases in vapor quality result in a slight decrease in the heat transfer coefficient, which is steeper at low vapor qualities. This figure also reveals an increasing heat transfer coefficient with increasing heat flux. In addition, it can be noted that the effect of mass velocity on α is marginal.

Table 1 Uncertainty of measured and calculated parameters

Parameter	Uncertainty
T_{in}, T_{out}	0.2°C
T_{wall}	0.4°C
p_{in}	1.0%
Mass velocity	2.1%
q at $q = 140$ kW/m^2	0.7%
q at $q = 370$ kW/m^2	0.5%
α at $\alpha = 15$ kW/m^{2}K	3.2%

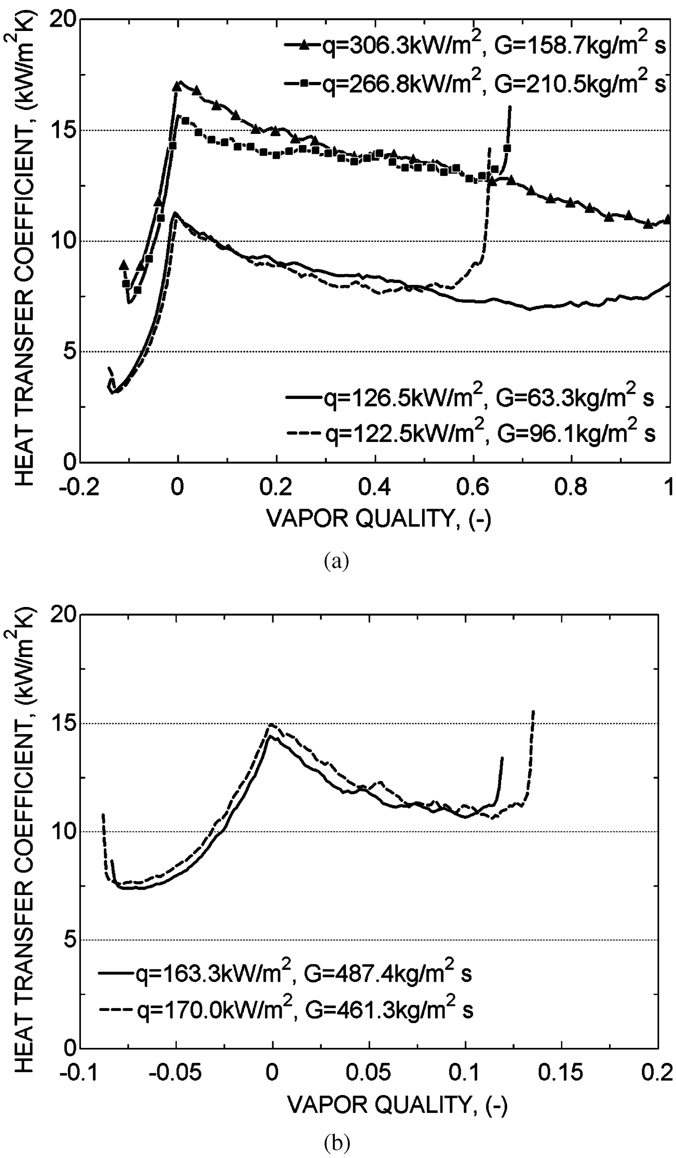

Figure 4 Heat transfer coefficients as a function of the local vapor quality (a) Low mass velocity and (b) High mass velocity.

The higher heat transfer coefficients at the extremities of the curves displayed in Figure 4 seem to be related to longitudinal conduction, which increases the estimated local heat transfer coefficient by decreasing the measured wall temperature. A two-dimensional finite differences analysis was performed to investigate these effects on the local heat flux in the region in contact with the fluid refrigerant, as well as on the temperature profile on the heating film. A rectangular surface (500 mm × 21.45 mm) was assumed to have an imposed heat flux through a total length of 16 mm centered on the lower face. Constant heat transfer coefficient on the upper face and uniform cooling fluid temperature were assumed. Adiabatic conditions were imposed on the remaining regions of the simulated heat sink. The results of these simulations and the variation on the experimental local heat transfer coefficient with the axial position are displayed in Figure 5.

Figure 5a shows that the experimental heat transfer coefficient increases at the extremes of the heating length. In Figure 5b, based on simulated results, it can be noted that the non-dimensional heat flux on the upper face of the heat sink, given as the ratio of the local heat flux to the applied heat flux on the lower face, decreases at the start and end of the heated length. A decrease in the wall temperature on the heating film side at both corners of the heated length is displayed in Figure 5c for experimental and simulated data. According to these results, the apparent increase in the heat transfer coefficient at the extremes of the heated section is due to a heat sink cooling length larger than the heating length. It can also be concluded that these effects are relevant just at the start and end of the heating length. Based on this discussion, the experimental heat transfer coefficient data considered in the present analysis were restricted to data obtained at saturated conditions and for z from 2 to 14 mm.

Finally, it should be mentioned that in the present study, an increase in the heat transfer coefficient with increasing x after a certain vapor quality due to the evaporation process itself observed by Xu et al. [14] was not displayed here despite the same experimental database. Such a difference is related to different data reduction procedures. Here, in the saturated region, a linear fluid temperature profile was adopted with the saturated fluid temperature decreasing along the channel due to pressure drop. On the other hand, Xu et al. [14] assumed a constant saturated fluid temperature at a pressure equal to the average between inlet and outlet values. Such a procedure over-predicts the saturation temperature at higher vapor qualities and, consequently, provides higher heat transfer coefficients. Axial conduction, inherent to the present test facility configuration, tends to amplify such a behavior by decreasing the wall temperatures at the end of the heated region. It is important to highlight that to estimate α, a local evaluation of the saturation temperature is needed due to the high pressure drops verified for evaporation in micro-scale channels. A linear profile, although not completely reflecting the variation of pressure and saturation temperature along the test section, appears to be a sound approach when lacking a well-established two-phase micro-channel pressure drop theory.

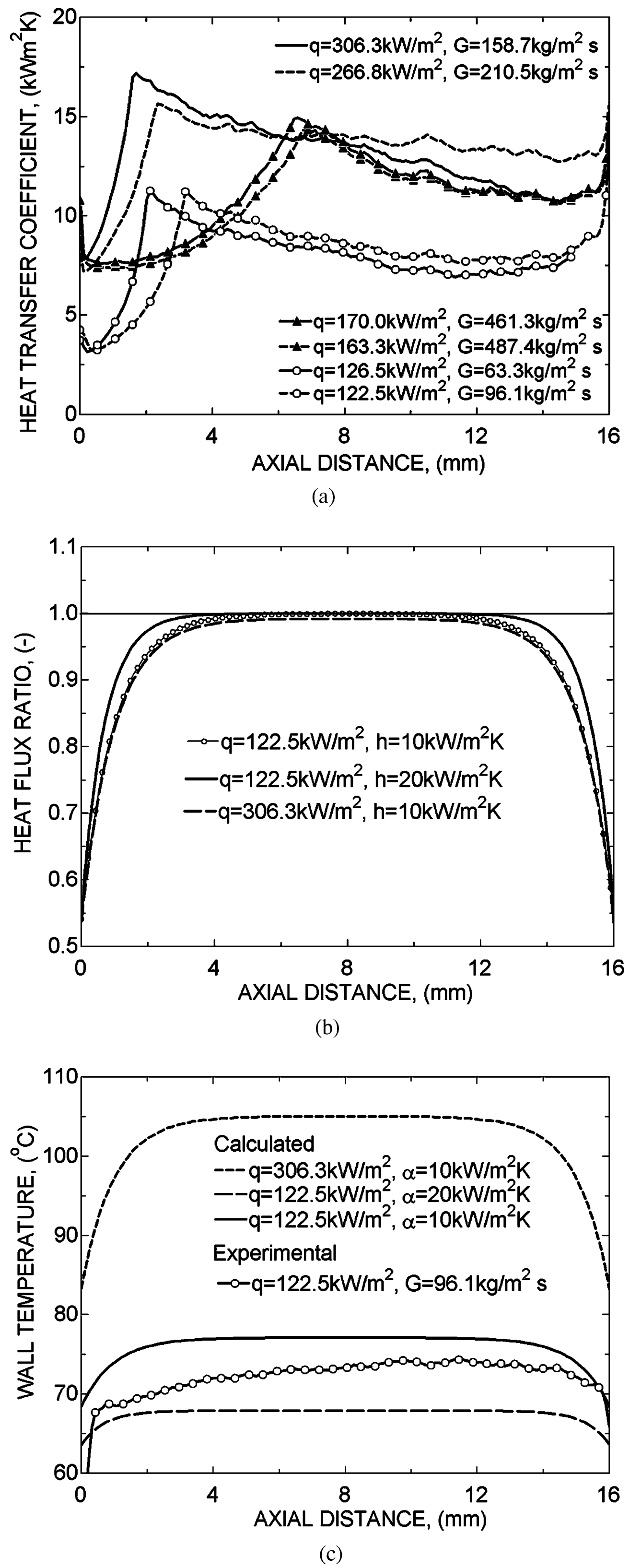

Figure 5 (a) Experimental heat transfer coefficient, (b) simulated ratio of the local heat flux on the cooled heat sink face and the applied heat flux on the lower face, (c) wall temperature on the heating film side as a function of the axial distance from the beginning of the heating length, z.

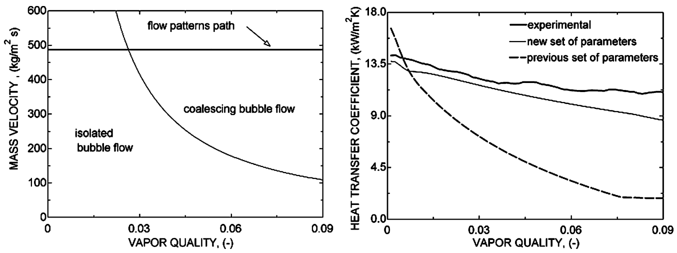

Figure 6 Flow pattern map plus experimental and predicted heat transfer coefficients as a function of vapor quality. $G = 487.4$ kg/m^2 s and $q = 163.3$ kW/m^2.

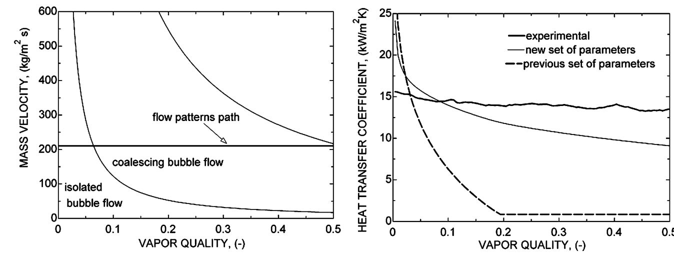

Figure 8 Flow pattern map plus experimental and predicted heat transfer coefficients as a function of vapor quality. $G = 210.5$ kg/m^2 s and $q = 266.8$ kW/m^2.

COMPARISON WITH THE THREE-ZONE MODEL AND DISCUSSION

By comparing the experimental heat transfer data segregated as isolated bubble flow and the three-zone model using the general set of parameters proposed by [12], it was found that the model predicts 69% of the present database within $\pm 30\%$. Statistically, this is a reasonable result, taking into account that both the heat transfer and the flow pattern prediction methods were developed for single channels and based on data for equivalent diameters larger than 0.83 mm and 0.5 mm, respectively. In addition, acetone was not included in the original database, which was mainly based on experimental results for halocarbon refrigerants. Figures 6–8 present flow pattern maps, illustrating the flow regime paths with increasing x, plus the respective heat transfer plots showing the evolution of α with vapor quality. In these figures, experimental and predicted heat transfer coefficients are presented. The empirical parameters proposed by [12] and new values optimized in this study were used to predict the heat transfer coefficient. The new values were optimized for the present heat transfer data segregated as isolated bubble flow and are presented in Table 2, where they are also compared against the original values proposed by [12]. It was found that using the new empirical parameters, the model predicts 90% of the isolated bubble flow heat transfer data within $\pm 30\%$ and 85% within $\pm 20\%$. Thus, the user of the three-zone model has the possibility to do general design and selection of the best heat fluid using the general values and can fit the model to a specific design/fluid combination if such data are available.

From the hypothesis presented in [2], it can be speculated that a lower $\delta_{\min}$ may be related to a lower surface roughness, as the present test section was fabricated by etching of a silicon wafer, which produces very smooth surfaces compared to metallic ones. Most of the databases in [12] cover experimental data in single tubes, probably manufactured by extrusion, which may result in rougher surfaces. The reason for a higher $C_{\delta 0}$ than the one proposed in [12] is not clear. A different channel configuration may be related to a higher initial film thickness. Therefore, despite the experimental difficulties, it seems obvious that the evaluation of the liquid film thickness in micro-scale channels is crucial in order to improve the predictive capability of the present model. The new values of c_q and n_f result in a lower bubble frequency than that resulting from the previous constants. A lower bubble frequency for acetone than for halocarbon refrigerants (most of the fluids considered in [12]) is in agreement with the frequency of bubble release at pool boiling conditions. Based on these aspects, it can be concluded that the effects related to the evaporating fluid on the bubble frequency are not well captured by the equation proposed to estimate τ in Eq. (2). Thus, this correlation should be improved by including in its fitting a larger number of fluids and a parameter characteristic of the fluid such as the molecular mass incorporated into the pool boiling correlation by Cooper [18].

According to Figures 6–8, when used with the empirical parameters by [12], the three-zone model gives a much steeper decrease in the heat transfer coefficient than the experimental data. In addition, within the coalescing bubble flow regime and at high enough vapor qualities, the heat transfer coefficient displays an elbow followed by a nearly invariant value. This is due to the fact that in the simulations t_{film} is set to 0 when δ_0 becomes smaller than δ_{end}. Such an assumption seems to be plausible because when this condition is achieved $\delta_0 = \delta_{end} = \delta_{\min}$ and film evaporation is not possible. Then, an almost constant heat transfer coefficient is obtained due to the fact that at this condition $L_l \ll L_v$ and thus an increase in α_l promoted by an increase in the triplet velocity with x has a negligible effect on the time-average

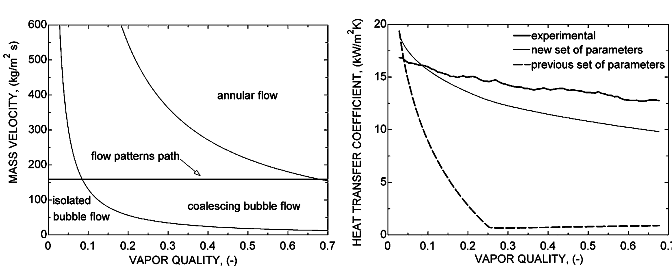

Figure 7 Flow pattern map plus experimental and predicted heat transfer coefficients as a function of vapor quality. $G = 158.7$ kg/m^2 s and $q = 306.3$ kW/m^2.

Table 2 Proposed values for the empirical parameters in the three-zone model

	$\delta_{\min}$ (m)	C_q (W/m^2 K)	n_q	n_f	$C_{\delta 0}$
Original empirical parameters values [12]	0.3×10^{-6}	3328	−0.5	1.74	0.29
Empirical parameters values obtained in the present study	0.1×10^{-6}	4653	−0.5	1.70	0.40

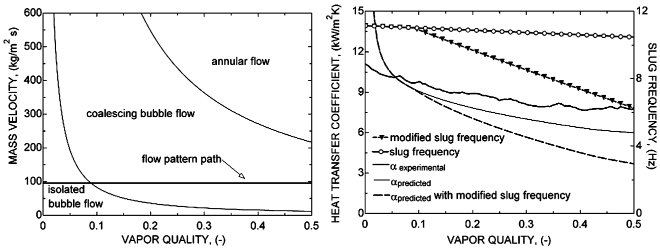

Figure 9 Illustration of the effect of the slug frequency taking into account flow patterns on the predicted heat transfer coefficient. $G = 96.1$ kg/m^2 s and $q = 122.5$ kW/m^2.

α, yielding an almost constant heat transfer coefficient. When using the new set of parameters, experimental and predicted results converge, and a condition of $t_{film} = 0$ is not achieved. In addition, it is important to highlight here that the peak in the heat transfer coefficient predicted by the three-zone model at a vapor quality at which the dry zone at the bubble tail starts was displayed by the present database just at subcooled conditions, and thus was not captured by the heat transfer model (which has not yet been extended to subcooled boiling conditions). It is also true that a small error in the experimental energy balance could have the effect of moving the peak to subcooled conditions.

The flow pattern maps displayed in Figures 6–8 show that isolated bubble flow occurs for narrow vapor quality ranges, with most of the flow being at the coalescing bubble regime. A bubble frequency being a function of the heat flux, as assumed in the three-zone model, is just verified for the isolated bubble flow. Based on these aspects, an analysis of the bubble/slug frequency effect on the heat transfer coefficient for a coalescing bubble flow was performed, the results of which are displayed in Figure 9. The following two different methods to calculate the bubble/slug frequency were adopted:

1. the bubble/slug frequency was calculated according to Eq. (2) for isolated bubble and coalescing bubble flows, as implemented for Figures 6–8; and
2. Eq. (2) was used to calculate the bubble/slug frequency at the isolated bubble flow followed by a linear variation in the frequency in the coalescing bubble flow mode, reaching a value of 0 Hz at the onset of annular flow.

The results shown in Figure 9 were calculated using the set of empirical parameters optimized in this study for acetone.

In Figure 9, the decrease in the predicted bubble/slug frequency calculated according to Eq. (2) is related to the diminishing saturation temperature along the channel length due to pressure drop. A value equal to 0 Hz for the modified slug frequency is not achieved in this figure because a transition to annular flow was not reached. In addition, a lower frequency given by the modified slug frequency results in a steeper decrease in the predicted heat transfer coefficient with increasing vapor quality, deteriorating the prediction of the experimental data. Here, under the light of the three-zone model, it can be speculated that as a consequence of the bubble collapse phenomenon, some liquid is trapped in the film region by the resulting elongated bubble. It could result in an evaporating film length for the new elongated bubble larger than the addition of the evaporating film lengths of the slugs before the collapse. Such a mechanism could counterbalance the effects of the decrease in the slug frequency, providing a smooth decrease in the heat transfer coefficient with vapor.

CONCLUSIONS

Heat transfer data for convective evaporation of acetone in a multi-channel micro-scale evaporator having triangular cross-section channels were compared against predictions by the three-zone model. The micro-scale flow pattern prediction method proposed by Revellin was used in order to utilize only test data corresponding to the elongated bubble flow mode. A data reduction procedure different from that used by Xu et al. was adopted here; thus, differences in the heat transfer coefficient behavior with x were found. Based on the experimental data segregated as isolated bubble flow, a new set of empirical parameters for the three-zone model was proposed that gave reasonable predictions. The conjugated effect of flow pattern and slug frequency on α was also investigated, and further research on this topic is suggested here.

NOMENCLATURE

C	specific heat, J/kg K
d	internal tube diameter, m
D_{eq}	equivalent diameter, m
G	mass velocity, kg/m^2 s
h_{lv}	latent heat of vaporization, J/kg
k	thermal conductivity, W/m K
L	length, m
L_h	heating length, m
p	pressure, kPa
p_{crit}	critical pressure, kPa
p_r	reduced pressure, p/p_{crit}, dimensionless
q	heat flux, W/m^2
Re	Reynolds number, $= Gd/\mu$, dimensionless
t	time, s
T	temperature, °C
x	vapor quality, dimensionless
z	distance from the beginning of the heating length, m

Greek Symbols

α	heat transfer coefficient, W/m^2 K
δ	liquid film thickness, m
μ	dynamic viscosity, kg/m s
ρ	density, kg/m^3
σ	surface tension, N/m

Subscripts

f	fluid
in	test section inlet
l	liquid
out	test section outlet
sat	saturation
v	vapor

REFERENCES

[1] Thome, J. R., Boiling in Microchannels: A Review of Experiments and Theory, *Int. J. Heat Fluid Flow*, vol. 25, pp. 128–139, 2004.

[2] Thome, J. R., Dupont, V., and Jacobi, A. M., Heat Transfer Model for Evaporation in Microchannels, Part I: Presentation of the Model, *Int. J. Heat Mass Transfer*, vol. 47, pp. 3375–3385, 2004.

[3] Ribatski, G., Wojtan, L., and Thome, J. R., An Analysis of Experimental Data and Prediction Methods for Two-Phase Frictional Pressure Drop and Flow Boiling Heat Transfer in Micro-Scale Channels, *Exp. Thermal Fluid Sci.*, vol. 31, pp. 1–19, 2006.

[4] Kandlikar, S. G., and Balasubramanian, P., An Extension of the Flow Boiling Correlation to Transition, Laminar, and Deep Laminar Flows in Minichannels and Microchannels, *Heat Transfer Eng.*, vol. 25, pp. 86–93, 2004.

[5] Zhang, W., Hibiki, T., and Mishima, K., Correlation for Flow Boiling Heat Transfer in Mini-Channels, *Int. J. Heat Mass Transfer*, vol. 47, pp. 5749–5763, 2004.

[6] Agostini, B., and Thome, J. R., Comparison of an Extended Database of Flow Boiling Heat Transfer Coefficient in Multi-Microchannel Elements with the Three-Zone Model, *Proc. ECI International Conference on Heat Transfer and Fluid Flow in Microscale*, Castelvecchio Pascoli, Italy, 2005.

[7] Agostini, B., Étude Expérimentale de l'Ebullition en Convection Forcée de Fluide Réfrigérant dans des Minicanaux, Ph.D. thesis, Université Joseph Fourier –Grenoble, France, 2002.

[8] Revellin, R., Experimental Two-Phase Fluid Flow in Microchannels, Ph.D. thesis, École Polytechnique Fédérale de Lausanne, Switzerland, 2005.

[9] *VDI-Wärmeatlas*, Springer-Verlag, Berlin, Heidelberg, 1997.

[10] Gnielinski, V., New Equations for Heat and Mass Transfer in Turbulent Pipe and Channel Flow, *Int. Chem. Eng.*, vol. 16, pp. 359–368, 1976.

[11] Churchill, S. W., and Usagi, R., A General Expression for the Correlation of Rates of Transfer and Other Phenomena, *AIChE Journal*, vol. 18, pp. 1121–1128, 1972.

[12] Dupont, V., Thome, J. R., and Jacobi, A. M., Heat Transfer Model for Evaporation in Microchannels, Part II: Comparison with the Database, *Int. J. Heat Mass Transfer*, vol. 47, pp. 3387–3401, 2004.

[13] Moriyama, K., and Inoue, A., Thickness of the Liquid Film Formed by a Growing Bubble in a Narrow Gap between Two Horizontal Plates, *J. Heat Transfer*, vol. 118, pp. 132–139, 1996.

[14] Xu, J. L., Shen, S., Gan, Y. H., Li, Y. X., Zhang, W., and Su, Q. C., Transient Flow Pattern Based Microscale Boiling Heat Transfer Mechanism, *J. Micromech. Microeng.,* vol. 15, pp. 1344–1361, 2005.

[15] Xu, J. L., Gan, Y. L., Zhang, D. C., and Li, X. H., Microscale Boiling Heat Transfer in a Micro-Timescale at High Heat Fluxes, *J. Micromech. Microeng*, vol. 15, pp. 362–376, 2005.

[16] Yaws, C. L., *Chemical Properties Handbook*, McGraw-Hill, New York, 1999.

[17] Shah, R. K., and London, A. L., Laminar Flow Forced Convection in Ducts, in *Advanced in Heat Transfer Supplement 1*, eds. T. F. Irvine, Jr. and J. P. Hartnett, Academic Press, New York, 1978.

[18] Cooper, M. G., Heat Flow Rates in Saturated Nucleate Pool Boiling—A Wide Ranging Examination Using Reduced Properties, *Adv. Heat Transfer*, vol. 16, pp. 157–238, 1984.

Gherhardt Ribatski is a post-doctoral researcher in the Laboratory of Heat and Mass Transfer at the Swiss Federal Institute of Technology in Lausanne (EPFL), Switzerland, since 2003. He received his B.Sc. in 1995, M.Sc. in 1998, and his Ph.D. in 2002, all in Mechanical Engineering from the University of São Paulo, Brazil. He was a post-doctoral researcher in the Department of Mechanical and Industrial Engineering at University of Illinois at Urbana-Champaign from 2002 to 2003. His research interests cover pool boiling, falling-film evaporation and condensation, two-phase flow, boiling and condensation of external and internal flow, and convective evaporation and condensation in micro-scale channels. He has published (or has in review) more than thirty papers on these subjects.

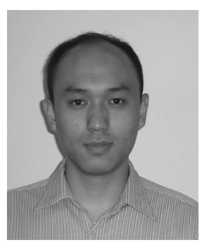

Wei Zhang received his B.S degree in Heating Ventilating & Air Conditioning Department of Tianjin University of Commerce, China, in 2001. He joined the Micro Energy System Laboratory, GIEC, CAS as a Ph.D. student in 2003. He has been working in the area of microfluidic and microscale heat transfer.

Lorenzo Consolini is a Ph.D. student in the Laboratory of Heat and Mass Transfer (LTCM) at the Swiss Federal Institute of Technology in Lausanne, Switzerland (EPFL). He received his Laurea degree in mechanical engineering at the University of Rome "Tor Vergata" and has a Master of Science degree from the University of Illinois at Chicago. At present, he is working on heat transfer aspects of convective boiling in microchannels.

Jinliang Xu is a professor and director of the Academic Committee of Guangzhou Institute of Energy Conversion, CAS, China. He is also the Director of the Basic Research Center and the Leader of the Micro Energy System Laboratory of the same institute. He has been working in the area of microfluidic and microscale heat transfer. He has more than twenty articles published in recognized international journals.

John R. Thome has been a professor of Heat and Mass Transfer at the Swiss Federal Institute of Technology in Lausanne (EPFL), Switzerland, since 1998, where his primary interests of research are two-phase flow and heat transfer cover boiling and condensation of internal and external flows, two-phase flow patterns and maps, experimental techniques on flow visualization and void fraction measurement, and more recently two-phase flow and boiling in microchannels. He received his Ph.D. from Oxford University, England, in 1978, and was formerly an assistant and associate professor at Michigan State University. He left in 1984 to set up his own international engineering consulting company. He is the author of three books: *Enhanced Boiling Heat Transfer* (Taylor & Francis, 1990), *Convective Boiling and Condensation* (Oxford University Press, 1994, 3rd ed. with J. G. Collier), and *Wolverine Engineering Databook III*, which is now available free from http://www.wlv.com/products/databook/db3/DataBookIII.pdf. He is now working on his fourth book. He received the ASME Heat Transfer Division's Best Paper Award in 1998 for a three-part paper on flow boiling heat transfer, published in the *Journal of Heat Transfer*. He also authored the chapter on boiling in the new *Heat Transfer Handbook* (2003). He has published (or has in review) more than 60 journal papers in the last six years on the topics of two-phase flow, boiling, and condensation in macro-scale and micro-scale flows, and is a frequent keynote speaker at international conferences. He is an associate editor of *Heat Transfer Engineering*.